

Scaling of normalized mean energy and scalar dissipation rates in a turbulent channel flow

Hiroyuki Abe^{1,a)} and Robert Anthony Antonia^{2,b)}

¹Japan Aerospace Exploration Agency, Tokyo 182-8522, Japan

²Discipline of Mechanical Engineering, University of Newcastle, Newcastle, New South Wales 2308, Australia

(Received 26 July 2010; accepted 6 April 2011; published online 25 May 2011)

Non-dimensional parameters for the mean energy and scalar dissipation rates C_ε and $C_{\varepsilon\theta}$ are examined using direct numerical simulation (DNS) data obtained in a fully developed turbulent channel flow with a passive scalar ($Pr = 0.71$) at several values of the Kármán (Reynolds) number h^+ . It is shown that C_ε and $C_{\varepsilon\theta}$ are approximately equal in the near-equilibrium region (viz., $y^+ = 100$ to $y/h = 0.7$) where the production and dissipation rates of either the turbulent kinetic energy or scalar variance are approximately equal and the magnitudes of the diffusion terms are negligibly small. The magnitudes of C_ε and $C_{\varepsilon\theta}$ are about 2 and 1 in the logarithmic and outer regions, respectively, when h^+ is sufficiently large. The former value is about the same for the channel, pipe, and turbulent boundary layer, reflecting the similarity between the mean velocity and temperature distributions among these three canonical flows. The latter value is, on the other hand, about twice as large as in homogeneous isotropic turbulence due to the existence of the large-scale u structures in the channel. The behaviour of C_ε and $C_{\varepsilon\theta}$ impacts on turbulence modeling. In particular, the similarity between C_ε and $C_{\varepsilon\theta}$ leads to a simple relation for the scalar variance to turbulent kinetic energy time-scale ratio, an important ingredient in the eddy diffusivity model. This similarity also yields a relation between the Taylor and Corrsin microscales and analogous relations, in terms of h^+ , for the Taylor microscale Reynolds number and Corrsin microscale Peclet number. This dependence is reasonably well supported by both the DNS data at small to moderate h^+ and the experimental data of Comte-Bellot [Ph. D. thesis (University of Grenoble, 1963)] at larger h^+ . It does not however apply to a turbulent boundary layer where the mean energy dissipation rate, normalized on either wall or outer variables, is about 30% larger than for the channel flow. © 2011 American Institute of Physics. [doi:10.1063/1.3584124]

I. INTRODUCTION

Over the past several decades, significant attention has been given to the mean energy dissipation rate,

$$\bar{\varepsilon} = \overline{vu_{ij}(u_{ij} + u_{j,i})}, \quad (1)$$

where u_1 , u_2 , and u_3 denote the streamwise, wall-normal, and spanwise velocity fluctuations, respectively; u , v , w are sometimes used interchangeably with u_1 , u_2 , u_3 ; ν denotes the kinematic viscosity and the overbar denotes averaging with respect to x , z (x , y , z denote the streamwise, wall-normal, and spanwise directions, respectively) and t (time), of the turbulent kinetic energy k ($\equiv \overline{u_i^2}/2$) owing to the dissipative nature of turbulence (see, for example, the pioneering work of Taylor¹ and Kolmogorov² and, more recently, the review of Sreenivasan and Antonia³). $\bar{\varepsilon}$ represents the rate at which the energy is dissipated at the molecular level. In statistically steady turbulence, this magnitude is equivalent to the rate of energy transfer from large to small scales in the energy cascade where it is classically assumed that eddies break up successively through inertial forces until their size becomes comparable to the Kolmogorov length scale

η ($\equiv (v^3/\bar{\varepsilon})^{1/4}$). This has led to the idea that $\bar{\varepsilon}$ should become independent of the viscosity in the limit of infinite Reynolds number, thus suggesting a non-dimensional parameter

$$C_\varepsilon = \bar{\varepsilon}\ell/v^3, \quad (2)$$

where v and ℓ denote the energy containing scales of velocity and length, respectively. This form was first addressed by Taylor;¹ it is sometimes referred to as the zeroth law of turbulence (e.g., Pearson *et al.*⁴); it is interpreted as the ratio of the kinetic energy v^2 to the corresponding time scale ℓ/v . To date, the possibility that the magnitude of C_ε becomes constant has been argued extensively in the literature (e.g., Batchelor,⁵ Sreenivasan,⁶⁻⁸ Lumley,⁹ Frisch,¹⁰ Kaneda *et al.*,¹¹ Antonia *et al.*,¹² Antonia and Pearson,¹³ Burattini *et al.*,¹⁴ and Goto and Vassilicos¹⁵). The constancy is also associated with the Re independence of the drag coefficient (Frisch¹⁰) and other turbulence modeling parameters, as mentioned below.

Following Eq. (2), the non-dimensional parameter,

$$C_\varepsilon = \bar{\varepsilon}L_{uu}/u'^3, \quad (3)$$

has been examined in detail in the wake of the seminal experimental work of Batchelor,⁵ where $\ell = L_{uu}$ and $v = u'$ (L_{uu} is the integral length scale of u and the prime denotes

^{a)}Electronic mail: habe@chofu.jaxa.jp.

^{b)}Electronic mail: robert.antonio@newcastle.edu.au.

the root-mean-square value). Unless otherwise stated, L_{uu} is hereafter defined as

$$L_{uu} = \int_0^\infty R_{uu}(r) dr, \quad (4)$$

where $R_{uu}(r) (\equiv \overline{u(x)u(x+r)}/u'^2)$ is the longitudinal two-point correlation of u . Sreenivasan⁷ collected a large body of experimental data for Eq. (3) in grid turbulence and pointed out that C_ε becomes constant when the Taylor microscale Reynolds number $R_{\lambda_1} (\equiv u'\lambda_1/\nu)$ is larger than 50 ($\lambda_1 (\equiv u'/u'_1)$ is the longitudinal Taylor microscale). Sreenivasan⁷ also evaluated C_ε in other turbulent flows, observing that the effects of shear and inhomogeneity are not negligible, viz., the magnitude of C_ε in either homogenous shear flows or inhomogeneous flows is not the same as in grid turbulence. In the latter context, Burattini *et al.*¹⁴ revisited the magnitude of C_ε in grid turbulence, two-dimensional wakes, and homogeneous shear flows. They noted that it exhibits a significant variation, typically in the range 0.5–2.5, for $R_{\lambda_1} > 50$. The previous studies suggest that the magnitude of C_ε becomes constant when R_{λ_1} is sufficiently large but that it depends on the type of flow. Even in the same flow, there is evidence to suggest that the magnitude can depend strongly on the initial conditions (e.g., Antonia *et al.*¹² and Antonia and Pearson¹³).

A significant amount of data for C_ε has also been obtained from direct numerical simulations (DNSs) of homogeneous isotropic turbulence. In the latter flow, L_{uu} is defined as

$$L_{uu} = \frac{\pi}{2u'^2} \int_0^\infty \frac{E(k)}{k} dk, \quad (5)$$

where $E(k)$ is the 3D energy spectrum and k the 3D wavenumber. From his survey of existing DNS data ($R_{\lambda_1} = 21$ –240), Sreenivasan⁸ indicated that while C_ε tends to become constant for $R_{\lambda_1} > 100$, its magnitude depends on how the turbulence is forced at low wavenumbers. Goto and Vassilicos¹⁵ varied this large-scale forcing systematically in their DNSs ($R_{\lambda_1} = 60.7$ –168). They observed that C_ε depends on the external force which sustains the turbulence independently of R_{λ_1} . Kaneda *et al.*¹¹ performed high resolution DNSs up to $R_{\lambda_1} = 1201$. They noted that while the magnitude of C_ε can vary with forcing for $R_{\lambda_1} < 250$, it tends to a constant value (0.4–0.5) at higher R_{λ_1} .

For the scalar field, some information has also been gleaned for the normalized parameter,

$$C_{\varepsilon\theta} = \overline{\varepsilon_\theta} \ell / \nu \phi^2, \quad (6)$$

based on the expectation that, like $\overline{\varepsilon}$, $\overline{\varepsilon_\theta}$ should become constant when $R_{\lambda_1} \rightarrow \infty$, where

$$\overline{\varepsilon_\theta} = \kappa \overline{\theta_{,i} \theta_{,i}} \quad (7)$$

is the mean scalar dissipation rate of the temperature variance $k_\theta (\equiv \theta^2/2)$ (κ is the thermal diffusivity and θ the temperature fluctuation) (e.g., Lumley,⁹ Xu *et al.*,¹⁶ Watanabe and Gotoh,¹⁷ and Donzis *et al.*¹⁸). By similarity to Eq. (3), the non-dimensional form

$$C_{\varepsilon\theta} = \overline{\varepsilon_\theta} L_{uu} / u' \theta'^2 \quad (8)$$

follows from (6) when $\ell = L_{uu}$, $\nu = u'$, and $\phi = \theta'$. Whilst $C_{\varepsilon\theta}$ may approach a constant at high R_{λ_1} , there is evidence to suggest that its magnitude depends on Pr ($\equiv \nu/\kappa$) (the molecular Prandtl number) or Sc (the Schmidt number) (Watanabe and Gotoh¹⁷ and Donzis *et al.*¹⁸) and initial conditions (Donzis *et al.*¹⁸) when R_{λ_1} is small.

In wall turbulence, $\overline{\varepsilon}$ and $\overline{\varepsilon_\theta}$ may also be described independently of the viscosity away from the wall. As for other turbulent flows, the most likely normalized parameters should be Eqs. (3) and (8) although other non-normalized forms may apply in the overlap (logarithmic) region. If it is assumed that $\ell = \kappa_u y$ and $\nu = u_\tau$ (u_τ and κ_u denote the friction velocity and the von Kármán constant, respectively), then

$$C_{\varepsilon EQ} = \overline{\varepsilon} y / u_\tau^3 = 1 / \kappa_u \quad (9)$$

(see also McKeon and Morrison¹⁹). Similarly, with $\ell = \kappa_\theta y$ and $\phi = T_\tau$ (T_τ and κ_θ denote the friction temperature and the von Kármán constant in the mean temperature distribution, respectively), we obtain

$$C_{\varepsilon\theta EQ} = \overline{\varepsilon_\theta} y / u_\tau T_\tau^2 = 1 / \kappa_\theta. \quad (10)$$

Equations (9) and (10) imply a relationship between the normalized parameters and the von Kármán constants. It should be noted that underpinning Eqs. (9) and (10) is the concept of local energy equilibrium (viz., $P_k = \overline{\varepsilon}$ and $P_\theta = \overline{\varepsilon_\theta}$) (P_k and P_θ are the mean production rates for k and k_θ). Experimentally, the latter assumption allows one to infer $\overline{\varepsilon}$ and $\overline{\varepsilon_\theta}$ indirectly (and accurately) from measured mean velocity and temperature distributions. It also leads to model parameters

$$C_D = C_\mu = u_\tau^4 / k^2 \quad (11)$$

in one- and two-equation models, viz.,

$$\overline{\varepsilon} = C_D \sqrt{k}^3 / \ell, \quad (12)$$

and the turbulent eddy viscosity,

$$\nu_t = C_\mu k^2 / \overline{\varepsilon}. \quad (13)$$

C_D and C_μ are hence associated with the normalized parameters; these magnitudes are often taken as 0.09 [this can also be estimated via Eq. (11)]. C_D and C_μ are also related to C_λ in the eddy diffusivity model

$$\kappa_t = c_\lambda (k^2 / \overline{\varepsilon}) R^p, \quad (14)$$

where

$$R = (k_\theta / \overline{\varepsilon_\theta}) / (k / \overline{\varepsilon}). \quad (15)$$

Note that R denotes the time scale ratio of the temperature variance $k_\theta / \overline{\varepsilon_\theta}$ to the turbulent kinetic energy $k / \overline{\varepsilon}$; near-wall damping functions are omitted in Eqs. (13) and (14). Nagano and Kim²⁰ used $p = 1/2$, while Yoshizawa²¹ used $p = 2$. Introducing the turbulent Prandtl number $Pr_t (\equiv \nu_t / \kappa_t)$ leads to a relationship between C_μ and C_λ , viz.,

$$Pr_t = (C_\mu/C_\lambda)R^{-p}. \quad (16)$$

Figure 1 suggests that energy equilibrium is indeed a better approximation for a turbulent channel flow than a turbulent boundary layer, thus implying that Eqs. (9) and (10) are better satisfied in the former flow. This also indicates that the magnitudes of C_ε and $C_{\varepsilon\theta}$ may not vary significantly in the equilibrium region of the channel since there is little spatial flux in the y direction. These normalized parameters, while essential for both physical and modeling aspects, are however yet to be examined comprehensively.

Direct numerical simulations, with good spatio-temporal resolution, have become indispensable for studying the properties of the small-scale turbulent motion. Most of the available DNS databases for wall-bounded flows have been for a turbulent channel flow, mainly due to the simple geometry of this flow. The relevant Reynolds number (or Kármán number) h^+ ($\equiv u_\tau h/\nu$; u_τ is the friction velocity and h the channel half-width; the superscript denotes normalization by wall variables) currently extends to 2000 (Hoyas and Jiménez²²). The

channel databases have also provided a wealth of information for the small scale characteristics of turbulence (e.g., Kim and Antonia²³ and Antonia and Kim²⁴). In the outer region, when Pr is close to unity, both ε (Blackburn *et al.*²⁵) and ε_θ (Abe *et al.*²⁶) isotropic turbulence both statistically and instantaneously (see also the spectral and physical analogy by Antonia *et al.*²⁷). There is also evidence that $\bar{\varepsilon}$ scales reasonably well on u_τ^3/y [viz., Eq. (9)] and u_τ^3/h in the logarithmic and outer regions, respectively (Hoyas and Jiménez²²).

Whilst several features of $\bar{\varepsilon}$ and $\bar{\varepsilon}_\theta$, including possible scaling laws, have been examined with the use of DNS data for a turbulent channel flow, the normalized parameters have yet to be tested rigorously. The main objective of this paper is to clarify the dependence on the distance from the wall and the Reynolds number of Eqs. (3) and (8) and the degree of similarity to other turbulent flows using our DNS databases (Abe *et al.*^{26,28}) with $Pr=0.71$. The relationships between Eqs. (3) and (9) and between Eqs. (8) and (10) will also be investigated. Particular attention is given to part of the outer region where viscous effects are small and energy equilibrium (viz., $P_k = \bar{\varepsilon}$ and $P_\theta = \bar{\varepsilon}_\theta$) represents a good approximation. It is hoped that the present investigation will shed some light on the scaling laws of $\bar{\varepsilon}$ and $\bar{\varepsilon}_\theta$ in the equilibrium region of a turbulent channel flow and should hence be useful for developing turbulence models [viz., Eqs. (12)–(14)] given the relationship between the normalized parameters and the model parameters.

The paper is organized as follows. The present DNS databases are described briefly in Sec. II. In Sec. III, the normalized energy and scalar dissipation rates [viz., Eqs. (3) and (8)] are examined across the channel, with an emphasis on the logarithmic and outer regions and the effect of L_{uu} on the magnitudes of C_ε and $C_{\varepsilon\theta}$. In Sec. IV, we consider how the normalized parameters relate to the time-scale ratio of the scalar variance to the turbulent kinetic energy R [viz., Eq. (15)] and a simple relationship between the longitudinal Taylor microscale λ_1 and the Corrsin microscale for the temperature fluctuation λ_θ ($\equiv \theta'/\theta'_1$) is proposed. In Sec. V, an attempt is made to formulate a dependence of R_{λ_1} and Pe ($\equiv u'\lambda_\theta/\kappa$) on h^+ in the outer region, using values of C_ε , $C_{\varepsilon\theta}$, u' , and L_{uu} . We also consider the applicability of the proposed form of R_{λ_1} to the turbulent boundary layer.

II. DNS DATABASES

The present DNS databases have been obtained from simulations with passive scalar transport by Abe *et al.*^{26,28} The flow is a fully developed turbulent channel flow driven by a constant mean streamwise pressure gradient. The passive scalar (temperature) is introduced through uniform heating from both walls. Four values of h^+ ($=180, 395, 640, \text{ and } 1020$) are used. The molecular Prandtl number (Pr) is 0.71.

The governing equations for the velocity and scalar fields consist of the Navier-Stokes and energy (conservation) equations, respectively. For the latter, a constant time-averaged heat-flux thermal boundary condition (Kasagi *et al.*²⁹) is used. This condition is sometimes referred to as the isoflux

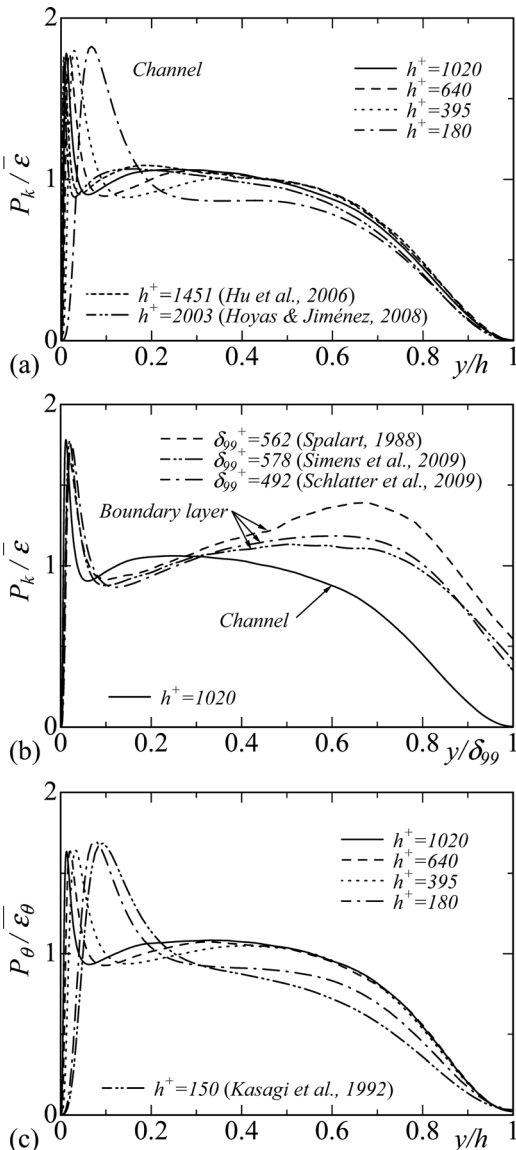


FIG. 1. Distributions of $P_k/\bar{\varepsilon}$ and $P_\theta/\bar{\varepsilon}_\theta$: (a), (b) $P_k/\bar{\varepsilon}$; (c) $P_\theta/\bar{\varepsilon}_\theta$.

TABLE I. Domain size, grid points, and spatial resolution.

h^+	180	395	640	1020
$L_x \times L_y \times L_z$	12.8h × 2h × 6.4h			
$L_x^+ \times L_y^+ \times L_z^+$	2304 × 360 × 1152	5056 × 790 × 2528	8192 × 1280 × 4096	13056 × 2040 × 6528
$N_x \times N_y \times N_z$	768 × 128 × 384	1536 × 192 × 768	2048 × 256 × 1024	2048 × 448 × 1536
$\Delta x^+, \Delta y^+, \Delta z^+$	3.00, 0.20–5.90, 3.00	3.29, 0.15–6.52, 3.29	4.00, 0.15–8.02, 4.00	6.38, 0.15–7.32, 4.25
$\Delta x_w^*, \Delta y_w^*, \Delta z_w^*$	1.94, 0.13, 1.94	2.24, 0.10, 2.24	2.77, 0.11, 2.77	4.46, 0.11, 2.97
$\Delta x_c^*, \Delta y_c^*, \Delta z_c^*$	0.82, 1.62, 0.82	0.74, 1.47, 0.74	0.82, 1.64, 0.82	1.16, 1.33, 0.77

condition, which is more realistic in experiments than the isothermal condition. Under the present condition, the bulk and wall mean temperatures increase linearly in the x direction, while the wall temperature fluctuation is assumed to be zero. This yields a relation

$$\frac{\partial \langle T^+ \rangle}{\partial x^\#} = \frac{\partial \langle T_m^+ \rangle}{\partial x^\#} = \frac{\partial \langle T_w^+ \rangle}{\partial x^\#} = \frac{2}{\int_0^2 \bar{U}_1 dy^\#} \quad (17)$$

for the present configuration (T , T_m , and T_w are the local, bulk, and wall temperatures, respectively; the angular bracket represents integration over z and t (time); the superscript # denotes the normalization by the channel half-width h [note that t is normalized by both u_τ and h]). In the simulations of Refs. 26 and 28, an instantaneous temperature difference Θ defined by

$$T = \frac{\partial \langle T_w \rangle}{\partial x} x - \Theta \quad (18)$$

is applied to the energy equation, which leads to the transformed energy equation expressed as

$$\frac{\partial \Theta^+}{\partial t^\#} + U_j^+ \frac{\partial \Theta^+}{\partial x_j^\#} = \frac{1}{h^+ \cdot Pr} \frac{\partial^2 \Theta^+}{\partial x_j^{\#2}} + U_i \frac{2}{\int_0^2 \bar{U}_1 dy^\#}, \quad (19)$$

where U_i is the instantaneous velocity in the i th direction (see also Ref. 29). The last term of Eq. (19) comes from relation (17) and plays a role in keeping the time-averaged heat-flux constant across the channel. As in the case of the Navier-Stokes equations, the no-slip and periodic boundary conditions are used for Eq. (19) in the y and other (x and z) directions, respectively.

The present thermal boundary condition differs only slightly from the internal source heating condition used by Kim and Moin.³⁰ In the latter case, the last term of Eq. (19) is set to be 2 so that the time-averaged heat-flux is not constant across the channel, although the wall temperature fluctuation is zero. Kasagi *et al.*²⁹ noted that basic turbulence statistics and turbulence structures obtained from these two simulations should be nearly identical.

The domain size ($L_x \times L_y \times L_z$), number of grid points ($N_x \times N_y \times N_z$), and spatial resolution (Δx , Δy , Δz) are given in Table I. Note that the superscript * represents normalization by either η , $v_K (\equiv (\nu \bar{\epsilon})^{1/4})$ (Kolmogorov velocity scale), or $\theta_B (\equiv (\bar{\epsilon}_\theta \nu^{1/2} \bar{\epsilon}^{-1/2})^{1/2})$ (Batchelor temperature scale) and the subscripts w and c refer to values at the wall and centerline, respectively. Since Pr is smaller than 1 in the present case, the Batchelor length scale, $\eta_B (\equiv \eta Pr^{-1/2})$, is slightly

larger than the Kolmogorov scale. The spatial resolution of the simulations is sufficient to describe adequately the behavior of all the scales of the flow up to the largest value of h^+ considered here (see also Abe *et al.*^{26,28} and Antonia *et al.*²⁷).

III. NORMALIZED ENERGY AND SCALAR DISSIPATION RATES

Figure 1 shows that there is an extended region, viz., $y^+ = 30$ to $y/h = 0.7$, where the ratios $P_k/\bar{\epsilon}$ and $P_\theta/\bar{\epsilon}_\theta$ are close to 1, at least when h^+ is sufficiently large (the DNS data in the present flow by Hoyas and Jiménez²² and Hu *et al.*³¹ for $P_k/\bar{\epsilon}$ and those by Kasagi *et al.*²⁹ for $P_\theta/\bar{\epsilon}_\theta$ are included for comparison). This region could therefore be interpreted as a region where energy equilibrium is validated approximately since the mean production and dissipation rates of the turbulent kinetic energy are approximately equal. Note that this region extends beyond that which is normally referred to as the log-law region. This seems to be associated with the presence of large-scale structures of u and θ spanning the channel where the intense sites of ϵ and ϵ_θ are most likely to coincide with the large-scale anisotropic u and θ structures, respectively (see, for example, Abe *et al.*²⁶ and Antonia *et al.*²⁷). Such an equilibrium region is less evident in a turbulent boundary layer (the DNS data for $P_k/\bar{\epsilon}$ of Spalart,³² Simens *et al.*,³³ and Schlatter *et al.*³⁴ are included in Fig. 1(b), where δ_{99} is used as the outer representative length scale). The difference appears to be mainly due to the importance of the advection term in the outer region of the boundary layer. This also implies that indirect estimates of $\bar{\epsilon}$ and $\bar{\epsilon}_\theta$ from P_k and P_θ would be less accurate in the latter flow.

In order to assess more precisely the extent of the equilibrium region, the magnitudes of the diffusion terms in the budgets of k and k_θ has also been examined. The transport equation of k , normalized by u_τ^4/ν , is written as

$$0 = \underbrace{-\overline{u_i^+ u_j^+} \frac{\partial \bar{U}_i^+}{\partial x_j^+}}_1 - \underbrace{\frac{\partial}{\partial x_j^+} \left(\frac{1}{2} \overline{u_i^{+2} u_j^+} \right)}_2 - \underbrace{\frac{\partial}{\partial x_j^+} \left(\frac{1}{2} \overline{u_i^+ p^+} \right)}_3 + \underbrace{\frac{\partial^2}{\partial x_j^{+2}} \left(\frac{1}{2} \overline{u_i^{+2}} \right)}_4 - \underbrace{\left(\frac{\partial u_i^+}{\partial x_j^+} \right)^2}_5, \quad (20)$$

where terms 1, 2, 3, 4, and 5 denote the production, turbulent diffusion, pressure diffusion, molecular diffusion, and homogeneous dissipation rate, respectively. Note that in Eq. (20), the homogeneous dissipation rate $\bar{\epsilon}_{\text{hom}}$ is used instead of the

full dissipation rate $\bar{\varepsilon}$. Also, the transport equation of k_θ , normalized by $u_\tau^2 T_\tau^2/\nu$, is

$$0 = \underbrace{-\overline{\theta^+ u_j^+} \frac{\partial \bar{\Theta}^+}{\partial x_j^+}}_1 + \underbrace{\overline{\theta^+ u_1^+} \frac{\partial \langle \bar{T}_m \rangle^+}{\partial x_1^+}}_2 - \underbrace{\frac{\partial}{\partial x_j^+} \left(\frac{1}{2} \overline{\theta^{+2} u_j^+} \right)}_3 + \underbrace{\frac{1}{Pr} \frac{\partial^2}{\partial x_j^{+2}} \left(\frac{1}{2} \overline{\theta^{+2}} \right)}_3 - \underbrace{\frac{1}{Pr} \left(\frac{\partial \theta^+}{\partial x_j^+} \right)^2}_4, \quad (21)$$

where terms 1, 2, 3, and 4 are the production, turbulent diffusion, molecular diffusion, and dissipation rate, respectively. Figure 2 displays that the turbulent and pressure diffusions are actually negligible only in the region $y^+ = 100$ to $y/h = 0.7$. It seems therefore more appropriate to refer to this latter region as a “near-equilibrium region.” With the exception of the latter region, the magnitudes of the diffusion terms are larger for Eq. (20) than for Eq. (21). In particular, the magnitude of the pressure diffusion term in Eq. (20), which is absent in Eq. (21), is appreciable for $y^+ < 100$. This suggests that the scalar field is closer to an equilibrium state than the velocity field over a wider range of the channel. It should also be noted that there is weak h^+ dependence on the diffusion terms for both Eqs. (20) and (21), which indicates that the region below $y^+ = 100$ is unlikely to be in energy equilibrium, at least for $h^+ = O(10^2) - (10^3)$.

Figure 3 indicates that C_ε [Eq. (3)] and $C_{\varepsilon\theta}$ [Eq. (8)] have nearly the same magnitude in the range $y^+ = 100$ to $y/h = 0.7$ (DNS (Hoyas and Jiménez²² and Hu *et al.*³¹) and

experimental (Comte-Bellot³⁵) data are also included) in which energy equilibrium is approximated closely. Note that when obtaining L_{uu} [Eq. (4)], the integration of R_{uu} has been carried out up to a separation which corresponds to the first zero crossing point (the extent of the integration is taken to $L_x/2$ when R_{uu} remains positive).

Outside the wall region, the magnitudes of C_ε and $C_{\varepsilon\theta}$ decrease significantly with increasing distance from the wall up to $y/h = 0.2$. Such y dependence may be explained via the distributions of $\bar{\varepsilon}h/u_\tau^3$, $\bar{\varepsilon}_\theta h/u_\tau T_\tau^2$, u'/u_τ , θ'/T_τ , and L_{uu}/h (Figs. 4–6) since

$$\bar{\varepsilon}L_{uu}/u^3 = (\bar{\varepsilon}h/u_\tau^3) \cdot (L_{uu}/h) \cdot (u_\tau^3/u^3), \quad (22)$$

$$\bar{\varepsilon}_\theta L_{uu}/u'\theta^2 = (\bar{\varepsilon}_\theta h/u_\tau T_\tau^2) \cdot (L_{uu}/h) \cdot (u_\tau/u') \cdot (T_\tau^2/\theta^2). \quad (23)$$

In that region, the magnitudes of $\bar{\varepsilon}h/u_\tau^3$ and $\bar{\varepsilon}_\theta h/u_\tau T_\tau^2$ are by one order larger than those of u'/u_τ , θ'/T_τ , and L_{uu}/h owing to the appreciable magnitudes of the mean velocity and temperature gradients. There is hence a similarity in shape between C_ε and $\bar{\varepsilon}h/u_\tau^3$ [viz., Figs. 3(a) and 4(a)] and between $C_{\varepsilon\theta}$ and $\bar{\varepsilon}_\theta h/u_\tau T_\tau^2$ [viz., Figs. 3(b) and 4(b)].

In the logarithmic region (viz., $y^+ = 100$ to $y/h = 0.2$), the values (~ 2) of C_ε and $C_{\varepsilon\theta}$ are nearly identical with those for $C_{\varepsilon EQ}$ [Eq. (9)] and $C_{\varepsilon\theta EQ}$ [Eq. (10)] (see insets of Fig. 4) and hence with κ_u^{-1} and κ_θ^{-1} . The same values of C_ε and $C_{\varepsilon EQ}$ are reported by Sreenivasan⁷ and McKeon and Morrison¹⁹ for a turbulent boundary layer and a turbulent pipe flow, respectively. It may thus be tempting to conclude that in the logarithmic region C_ε and $C_{\varepsilon\theta}$ are identical for these three canonical flows. This equality appears to be associated with the similarity between the mean velocity and temperature distributions.

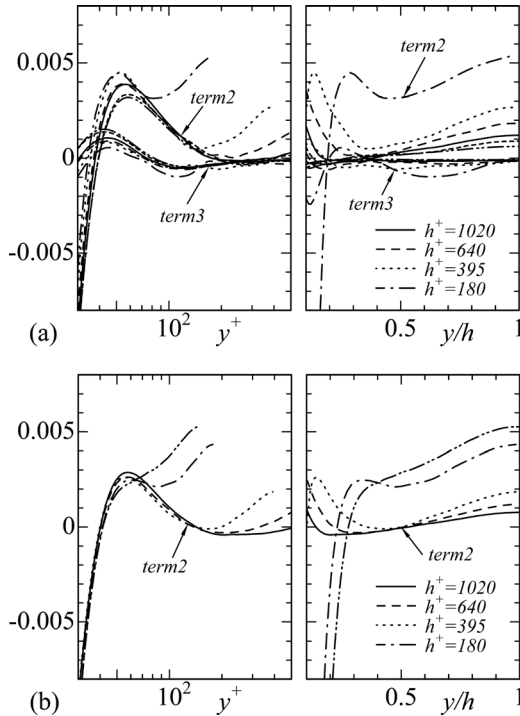


FIG. 2. Distributions of the diffusion terms in the budgets of k and k_θ normalized on inner variables: (a) terms 2 and 3 in Eq. (20); (b) term 2 in Eq. (21). In (a), - - - -, $h^+ = 1451$ [Hu *et al.* (Ref. 31)]; - · - · - ·, $h^+ = 2003$ [Hoyas and Jiménez (Ref. 22)], while in (b), - · - · - ·, $h^+ = 150$ [Kasagi *et al.* (Ref. 29)].

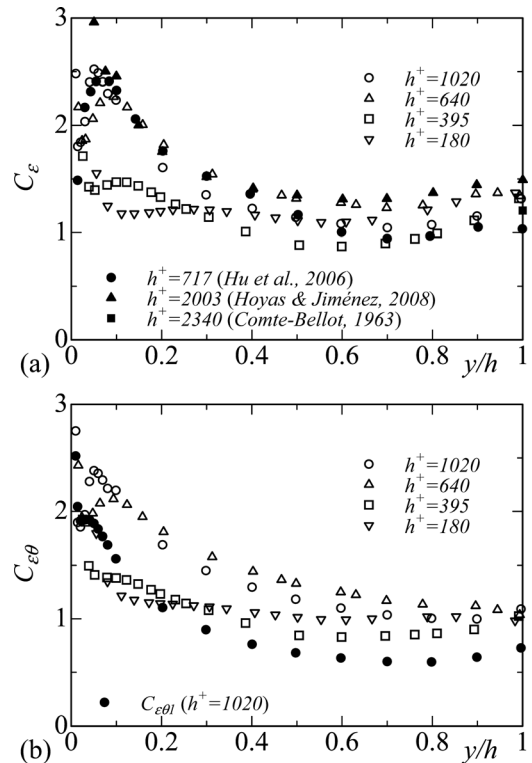


FIG. 3. Distributions of C_ε and $C_{\varepsilon\theta}$: (a) C_ε ; (b) $C_{\varepsilon\theta}$.

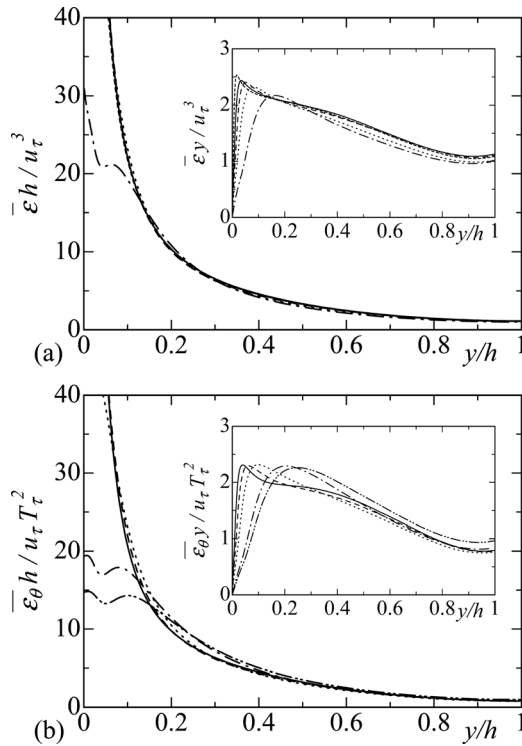


FIG. 4. Distributions of $\bar{\epsilon}h/u_\tau^3$ (a) and $\bar{\epsilon}_\theta h/u_\tau T_\tau^2$ (b) where the insets (a) and (b) show the distributions of $\bar{\epsilon}y/u_\tau^3$ and $\bar{\epsilon}_\theta y/u_\tau T_\tau^2$, respectively. —, $h^+ = 1020$; ---, $h^+ = 640$; ·····, $h^+ = 395$; — · — ·, $h^+ = 180$; - - - - -, $h^+ = 2003$ [Hoyas and Jiménez (Ref. 22)]; — · — · — ·, $h^+ = 150$ [Kasagi *et al.* (Ref. 29)].

For $0.3 < y/h < 0.7$, the variations of C_ϵ and $C_{\epsilon\theta}$ are small and their magnitudes are close to 1. This latter value is however about twice as large as in homogeneous isotropic turbulence (Sreenivasan,⁸ Kaneda *et al.*,¹¹ Watanabe and Gotoh,¹⁷ and Donzis *et al.*¹⁸). This is most likely associated with the existence of large-scale u structures in the outer region since L_{uu}/h exhibits a nearly parabolic distribution with a tendency to a plateau (~ 1) [see Fig. 6(a)], although the magnitudes of $\bar{\epsilon}h/u_\tau^3$, $\bar{\epsilon}_\theta h/u_\tau T_\tau^2$, u'/u_τ , and θ'/T_τ decrease monotonically (see Figs. 4 and 5).

The spread in the magnitudes of C_ϵ and $C_{\epsilon\theta}$ most probably reflects the difficulty in determining L_{uu} accurately. Although the large-scale structures ($\sim 3h$) should be adequately resolved by the current DNSs, very large-scale structures with a length scale larger than $25h$ (Hutchins and Marusic³⁶ and Monty and Chong³⁷) are unlikely to be captured correctly. To gain further insight into this, we have integrated the two-point correlation of u for two different intervals, viz.,

$$L_{uu1} = \int_0^{3h} R_{uu}(r)dr, \quad (24)$$

$$L_{uu2} = \int_{3h}^{L_x/2} R_{uu}(r)dr, \quad (25)$$

where L_{uu1} and L_{uu2} correspond to the contributions from the large-scale structures and the very-large-scale structures, respectively. Figure 6 suggests that while the level of L_{uu1} increases slowly with h^+ in the outer region, L_{uu2} exhibits a

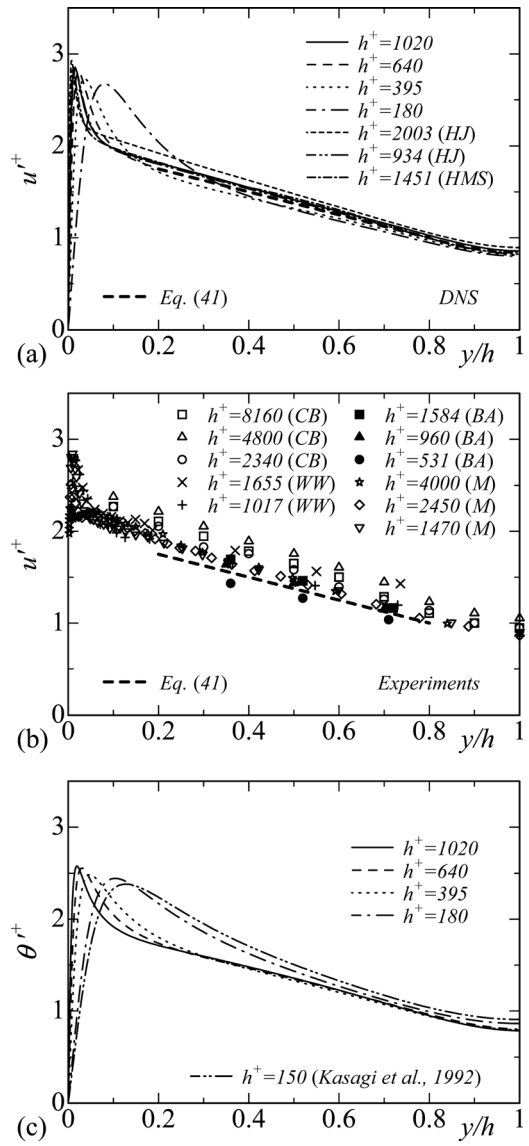
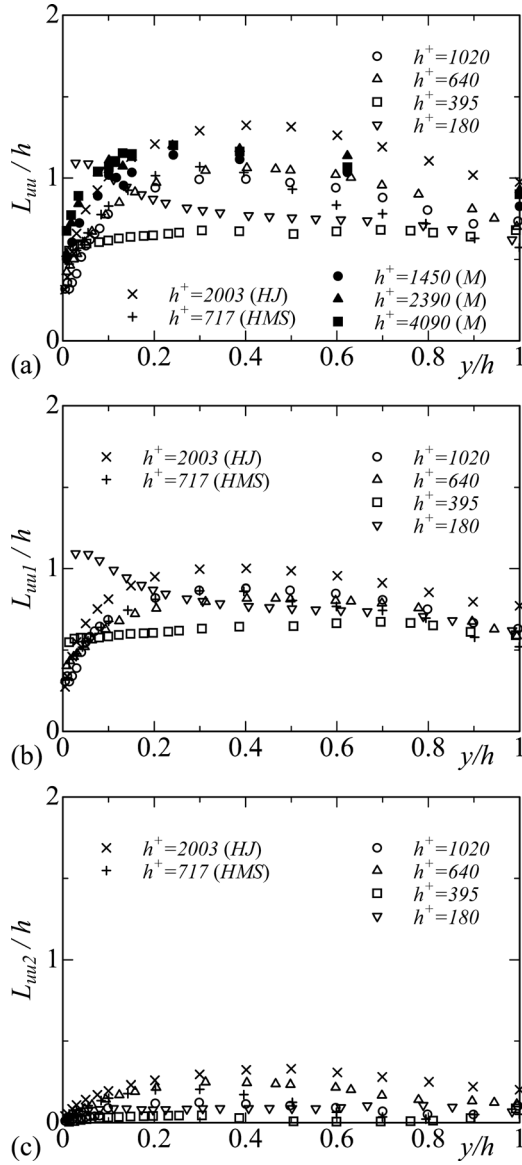


FIG. 5. Distributions of u^+ and θ^+ : (a), (b) u^+ ; (c) θ^+ .

large spread. The latter is associated with the difficulty in obtaining the data at large separations accurately, presumably reflecting the insufficiency of either the computational domain size or the sampling time period.

The effects of $R_{\lambda 1}$ and the Kolmogorov-normalized mean shear $S^*(\equiv d\bar{U}^*/dy^*)$ may not be entirely dismissed in the context of the magnitudes for C_ϵ and $C_{\epsilon\theta}$. In the present flow, the magnitudes of $R_{\lambda 1}$ and S^* do not depend noticeably on y/h for a particular value of h^+ in the near-equilibrium region. For a given value of y/h , $R_{\lambda 1}$ increases whilst S^* decreases as h^+ increases. At $y/h = 0.4$, where $R_{\lambda 1}$ exhibits a local maximum [see Fig. 11(a)], the magnitude of $R_{\lambda 1}$ increases monotonically from 62 ($h^+ = 180$) to 149 ($h^+ = 1020$), whilst that of S^* decreases systematically from 0.23 ($h^+ = 180$) to 0.12 ($h^+ = 1020$). From the previous observations, one may infer that, in the present flow, the effect of $R_{\lambda 1}$ and S^* on the magnitudes of C_ϵ and $C_{\epsilon\theta}$ should be less important than that of L_{uu} .

In the latter context, replacing L_{uu} by $L_{\theta\theta}$ in Eq. (8) yields

FIG. 6. Distributions of L_{uu}/h : (a) L_{uu}/h ; (b) L_{uu1}/h ; (c) L_{uu2}/h .

$$C_{\varepsilon\theta 1} = \overline{\varepsilon_\theta} L_{\theta\theta} / u' \theta^2, \quad (26)$$

where

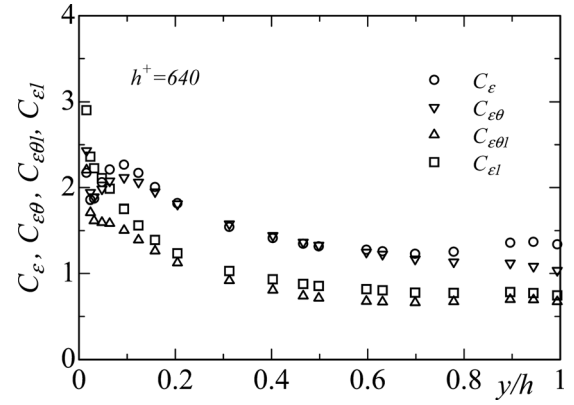
$$L_{\theta\theta} = \int_0^\infty R_{\theta\theta}(r) dr. \quad (27)$$

This reduces the magnitude by a factor of about two [see the difference between $C_{\varepsilon\theta}$ and $C_{\varepsilon\theta 1}$ in Fig. 3(b)], reflecting the smaller extent of the large-scale θ structures relative to the large-scale u structures (see Antonia *et al.*²⁷).

In the context of forming C_ε , there are advantages in replacing L_{uu} by L_{qq} , viz.,

$$L_{qq} = \int_0^\infty R_{uu}(r) dr + \int_0^\infty R_{vv}(r) dr + \int_0^\infty R_{ww}(r) dr, \quad (28)$$

where $q^2 \equiv u_i^2$. Antonia *et al.*²⁷ reported that the analogy, in both spectral and physical spaces, between \mathbf{q} (the fluctuating velocity vector) and θ holds reasonably well throughout the

FIG. 7. Distributions of C_ε , $C_{\varepsilon\theta}$, $C_{\varepsilon 1}$, and $C_{\varepsilon\theta 1}$ at $h^+ = 640$.

channel when Pr is close to unity. This analogy suggests another possible form for the normalized mean energy dissipation rate, viz.,

$$C_{\varepsilon 1} = \overline{\varepsilon} L_{qq} / u' q^2. \quad (29)$$

A comparison between $C_{\varepsilon 1}$ and $C_{\varepsilon\theta 1}$ along with that between C_ε and $C_{\varepsilon\theta}$ is made at $h^+ = 640$ and is shown in Fig. 7. Like C_ε and $C_{\varepsilon\theta}$, the normalized parameters are in closer agreement when L_{qq} and $L_{\theta\theta}$ are used in conjunction with q^2 and θ^2 (viz., $C_{\varepsilon 1}$ and $C_{\varepsilon\theta 1}$) in the near-equilibrium region. The present result reflects the reasonable similarity between q^2 and θ^2 . Note that the variation of $L_{\theta\theta}/L_{qq}$ is small across the channel [Fig. 9(c)], which is another consequence of the excellent analogy between \mathbf{q} and θ .

From a turbulence modeling viewpoint, it is worth enquiring into the difference between the magnitude of L_{uu} and that of the mixing length L_m ($L_m = \kappa_\mu y$ near the wall, while $L_m = 0.1h$ in the outer region). In the present flow, the mixing length is more likely to be identifiable with the dissipation length scale

$$L_\varepsilon = (-\overline{u\bar{v}})^{3/2} / \overline{\varepsilon} \quad (30)$$

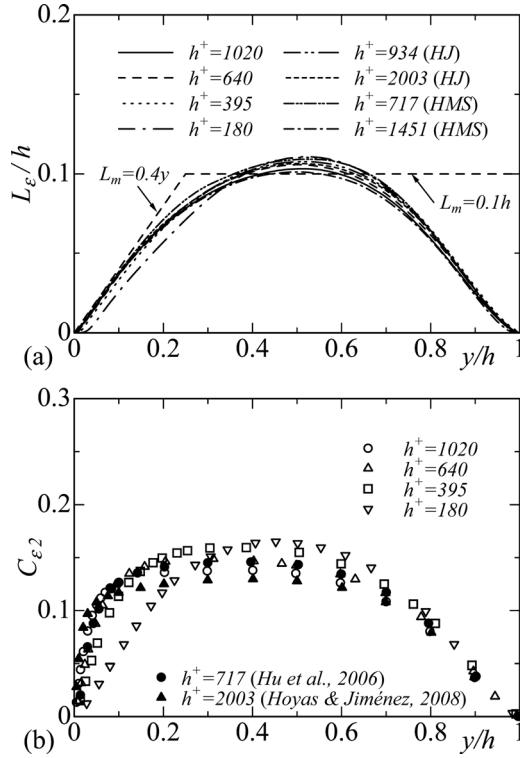
[Fig. 8(a)] than with L_{uu} [Fig. 6(a)]. Bradshaw³⁸ also suggested that the magnitude of L_m is nearly equal to that of L_ε across most of the boundary layer. After substituting L_ε and \sqrt{k} for ℓ and v , respectively, in Eq. (2), we obtain another normalized parameter, viz.,

$$C_{\varepsilon 2} = \overline{\varepsilon} L_\varepsilon / \sqrt{k}^3, \quad (31)$$

this relation being identical with Eq. (12). Figure 8(b) shows that $C_{\varepsilon 2} \sim 0.1$ over the equilibrium region. This value is not far from $C_D = C_\mu = 0.09$ in the model calculations, which leads to reasonable model predictions in the present flow.

IV. RELATIONSHIP BETWEEN THE NORMALIZED PARAMETERS AND TIME SCALE RATIO

The approximate equality of C_ε and $C_{\varepsilon\theta}$ in the region $y^+ = 100$ to $y/h = 0.7$ has important implications for the time scale ratio R . By substituting Eqs. (3) and (8) into Eq. (15), we obtain


 FIG. 8. Distributions of L_{ϵ}/h and $C_{\epsilon 2}$: (a) L_{ϵ}/h ; (b) $C_{\epsilon 2}$.

$$R = \frac{\overline{uu} C_{\epsilon 1}}{\overline{qq} C_{\epsilon \theta 1}}. \quad (32)$$

Also, the near equality of $C_{\epsilon 1}$ [Eq. (29)] and $C_{\epsilon \theta 1}$ [Eq. (26)] in this region leads to an alternative form

$$R = \frac{L_{\theta\theta} C_{\epsilon 1}}{L_{qq} C_{\epsilon \theta 1}}. \quad (33)$$

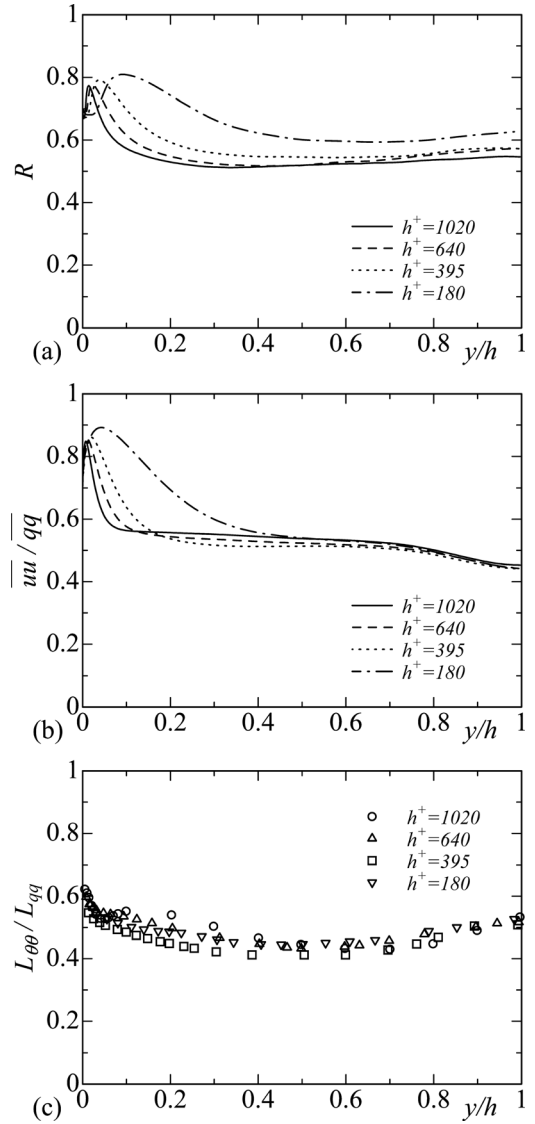
Since $C_{\epsilon} \simeq C_{\epsilon \theta}$ and $C_{\epsilon 1} \simeq C_{\epsilon \theta 1}$ in this range, R may be approximated in two different ways

$$R = \overline{uu}/\overline{qq} \quad (34)$$

and

$$R = L_{\theta\theta}/L_{qq}. \quad (35)$$

Equations (34) and (35) are tested against the DNS data in Fig. 9, which indicates that these equations are reasonable approximations to R over the region $y^+ = 100$ to $y/h = 0.7$ (one exception is $h^+ = 180$ due to the low Reynolds-number effects) for $Pr = 0.71$. The magnitude of R , however, increases slowly with increasing Pr in the outer region (see Kasagi and Ohtsubo,³⁹ Kawamura *et al.*,^{40,41} Schwertfirm and Manhart,⁴² and Kozuka *et al.*⁴³); for $h^+ = 395$, R varies from 0.1 ($Pr = 0.025$) to 1 ($Pr = 10$). This needs to be incorporated into Eq. (34) when formulating R . The latter formula may allow us to exclude R from Eq. (14). This may be desirable for developing the eddy diffusivity model since the inclusion of the scalar time scale in Eq. (14) violates the linearity principle of the scalar transport (Pope⁴⁴).


 FIG. 9. Distributions of R , $\overline{uu}/\overline{qq}$, and $L_{\theta\theta}/L_{qq}$: (a) R ; (b) $\overline{uu}/\overline{qq}$; (c) $L_{\theta\theta}/L_{qq}$.

Equation (34) also suggests the existence of a possible relationship between λ_1 and λ_θ . Assuming isotropic forms for $\bar{\epsilon}$ and $\bar{\epsilon}_\theta$, R may be written as

$$R = 5Pr \frac{\overline{uu}}{\overline{qq}} \left(\frac{\lambda_\theta}{\lambda_1} \right)^2. \quad (36)$$

Substituting Eq. (34) into Eq. (36) leads to

$$\lambda_\theta = \lambda_1 / \sqrt{5Pr}. \quad (37)$$

This relation may be useful for estimating λ_θ , although the Prandtl-number effect on R is expected to affect the prediction of Eq. (37) to some extent. This is tested in Fig. 10 where the DNS channel flow data of Kozuka *et al.*⁴³ ($h^+ = 395$ and $Pr = 2$ and 10) and Abe *et al.*²⁸ ($h^+ = 395$ and $Pr = 0.025$) are included to clarify the Prandtl-number dependence. The isotropic form $\lambda_{\theta iso} (\equiv \theta' / \sqrt{\bar{\epsilon}_\theta / 3\kappa})$ is also used; the isotropic relation is reasonable in the outer region, consistent with the results of Antonia *et al.*²⁷ for $\bar{\epsilon}_{iso}$ and $\bar{\epsilon}_{\theta iso}$, except for $h^+ = 180$ due to the low Reynolds-number effects [see Fig. 10(a)]. In the near-equilibrium region,

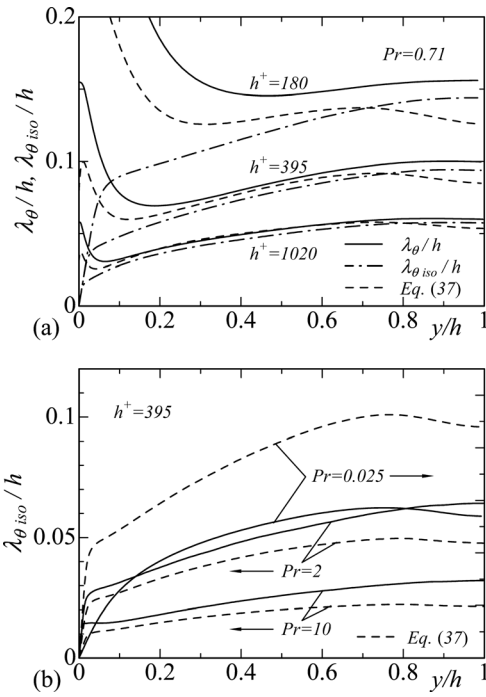


FIG. 10. Distributions of $\lambda_{\theta}h$ and $\lambda_{\theta_{iso}}h$: (a) $\lambda_{\theta}h$ and $\lambda_{\theta_{iso}}h$ for $Pr=0.71$; (b) $\lambda_{\theta_{iso}}h$ for $h^+=395$.

Eq. (37) is not applicable for $Pr=0.025$ (viz., mercury) but is likely to be valid at least for $Pr=0.71-10$ (viz., air and water), the latter Pr range being larger than that for Eq. (34). This finding is of importance for formulating Pe , as discussed in Sec. V.

V. FORMULATIONS FOR R_{λ_1} AND Pe

Empirical expressions for the dependence on h^+ of R_{λ_1} and Pe in a part of the outer region (viz., $0.3 < y/h < 0.7$) can be established with the use of the approximate equality between C_ε and $C_{\varepsilon\theta}$ in this range. With the use of the approximation $C_\varepsilon = C_{\varepsilon\theta} = 1.2$ and $L_{uu}/h = 1.2$ and the assumption of local isotropy, R_{λ_1} and Pe may be expressed as

$$R_{\lambda_1} = \frac{u'\lambda_1}{\nu} = \sqrt{u'^+} \cdot \sqrt{\frac{15}{C_\varepsilon}} \cdot \sqrt{\frac{L_{uu}}{h}} \cdot \sqrt{h^+} \approx 3.9\sqrt{u'^+h^+} \quad (38)$$

and

$$Pe = \frac{u'\lambda_\theta}{\kappa} = \sqrt{u'^+} \cdot \sqrt{\frac{3}{C_{\varepsilon\theta}}} \cdot \sqrt{\frac{L_{uu}}{h}} \cdot \sqrt{h^+Pr} \approx 1.7\sqrt{u'^+h^+Pr}, \quad (39)$$

where u'^+ depends on y . Note that Eqs. (38) and (39) yield

$$Pe = \sqrt{Pr/5}R_{\lambda_1}, \quad (40)$$

which is analogous to the previously obtained relationship between λ_1 and λ_θ , viz., Eq. (37).

Our DNS databases ($180 \leq h^+ \leq 1020$) suggest that u'^+ can be approximated by

$$u'^+ = -1.25(y/h) + 2 \quad (41)$$

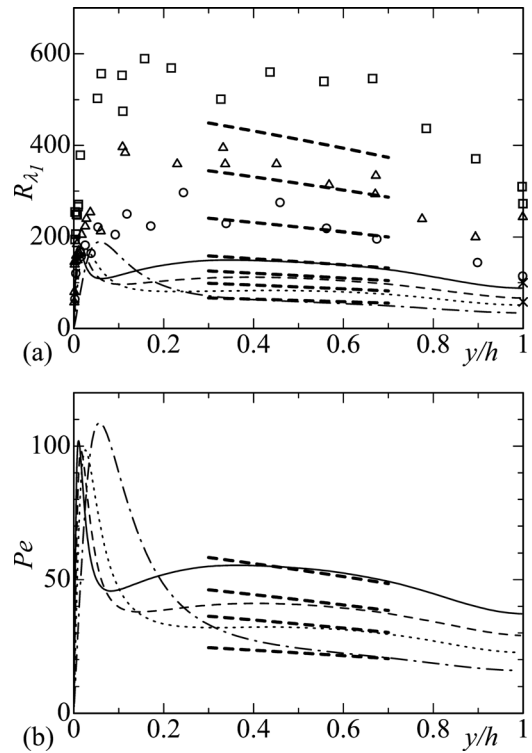


FIG. 11. Formulations for R_{λ_1} [Eq. (38)] and Pe [Eq. (39)] in the region $0.3 < y/h < 0.7$: (a) R_{λ_1} ; (b) Pe : —, $h^+=1020$; ---, $h^+=640$; , $h^+=395$; - · - · - , $h^+=180$; - - - - , predictions. Symbols denote the experimental data of Comte-Bellot (Ref. 35): \circ , $h^+=2340$; \triangle , $h^+=4800$; \square , $h^+=8160$.

[see Fig. 5(a)]. While a more rigorous form may be obtained by including Reynolds-number effects, Eq. (41) is reasonable at least for $h^+ = O(10^2) \sim (10^3)$. With regard to the distributions of u'^+ , a discernible difference may be noticed between the DNS [Hoyas and Jiménez²² (HJ)] and experimental [Comte-Bellot³⁵ (CB)] data at a comparable h^+ . This discrepancy may be due to u_τ being underestimated in CB's measurements since her distributions of \bar{U}^+ (not shown here) and u'^+ [Fig. 5(a)] for the lowest h^+ are about 8% larger than those of HJ in the outer region. For the highest h^+ of the CB data, the effect of compressibility may not be dismissed. It should also be noted that whilst the magnitude of u'^+ seems to increase slowly with h^+ in the outer region, the measurements do not always indicate consistent trends for $h^+ > 1000$; CB and WW (Wei and Willmarth⁴⁵) report larger magnitudes than BA (Balakumar and Adrian⁴⁶) and M (Monty⁴⁷), while the distributions of BA, M, and HMS (Hu *et al.*³¹) are close to each other at a comparable h^+ .

Equations (38) and (39) are tested in the region $0.3 < y/h < 0.7$ in Fig. 11. For both R_{λ_1} and Pe , the agreement between these predictions and the DNS data is satisfactory. The poor agreement with the CB data particularly for her largest h^+ seems to be due to the limited spatial resolution of the hot wire. This attenuates small-scale intensities significantly (Hutchins *et al.*⁴⁸) and would lead to an underestimation of u'_1 (viz., $\bar{\varepsilon}$) and an artificial increase in λ_1 (viz., R_{λ_1}).

We focus here on the behaviors of R_{λ_1} and Pe at $y/h = 0.4$ where R_{λ_1} and Pe exhibit local maxima (see Fig. 11). At this location, Eqs. (38) and (39) can be rewritten as

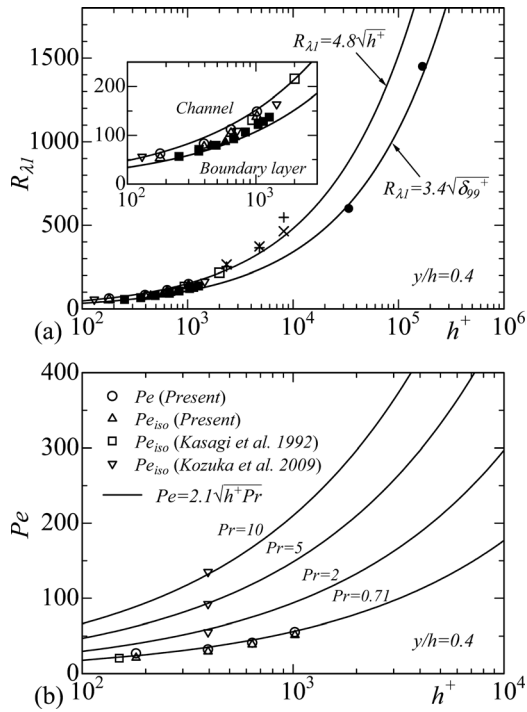


FIG. 12. Formulations for $R_{\lambda 1}$ [Eqs. (42) and (44)] and Pe [Eq. (43)] at $y/h = 0.4$: (a) $R_{\lambda 1}$; (b) Pe . In (a), \circ , $R_{\lambda 1}$ (Present); \triangle , $R_{\lambda 1iso}$ (Present); \square , $R_{\lambda 1iso}$ [Hoyas and Jiménez (Ref. 22)]; ∇ , $R_{\lambda 1iso}$ [Hu *et al.* (Ref. 31)]; $+$, $R_{\lambda 1}$ [Comte-Bellot (Ref. 35)]; \times , $R_{\lambda 1}$ [Comte-Bellot (Ref. 35)] for which the correction was made; \bullet , $R_{\lambda 1}$ [Saddoughi and Veeravalli (Ref. 49)]; \blacktriangle , $R_{\lambda 1iso}$ [Simens *et al.* (Ref. 33)]; \blacksquare , $R_{\lambda 1iso}$ [Schlatter *et al.* (Ref. 34)].

$$R_{\lambda 1} = 4.8\sqrt{h^+} \quad (42)$$

and

$$Pe = 2.1\sqrt{h^+ Pr}. \quad (43)$$

The predictions of Eqs. (42) and (43) are shown in Fig. 12; the data for $R_{\lambda 1iso}$ ($\equiv u' \lambda_{1iso} / \nu$) and Pe_{iso} ($\equiv u' \lambda_{0iso} / \kappa$) are also included in Fig. 12. Note that $\lambda_{1iso} \equiv u' / \sqrt{\bar{\epsilon}} / 15\nu$. The predicted values are in close agreement with the DNS data; there is only a small difference between $R_{\lambda 1}$ and $R_{\lambda 1iso}$ and also between Pe and Pe_{iso} . The magnitudes of $R_{\lambda 1}$ originally given by CB are slightly larger than the predictions of Eq. (42) especially for her highest h^+ . The CB data, however, become closer to the present predictions when a correction is applied for λ_1 based on the assumption $P_k = \bar{\epsilon}$. For Pe , the Prandtl-number effect seems to be reproduced reasonably well for $Pr = 0.71$ –10, consistently with the results for λ_θ [see also Fig. 10(b)].

It seems appropriate to enquire if Eqs. (42) and (43) apply to other wall-bounded flows. The boundary layer measurements of Saddoughi and Veeravalli⁴⁹ at $\delta_{99}^+ = 3.4 \times 10^4$ ($y/\delta_{99} \approx 0.5$) and 1.7×10^5 ($y/\delta_{99} \approx 0.4$) indicate that Eq. (42) overestimates $R_{\lambda 1}$ by about 30%; the latter values seem to be approximated by

$$R_{\lambda 1} = 3.4\sqrt{\delta_{99}^+} \quad (44)$$

[see Fig. 12(a)]. The data for $R_{\lambda 1iso}$ by Simens *et al.*³³ ($\delta_{99}^+ = 445$ –690) and Schlatter *et al.*³⁴ ($\delta_{99}^+ = 252$ –1271)

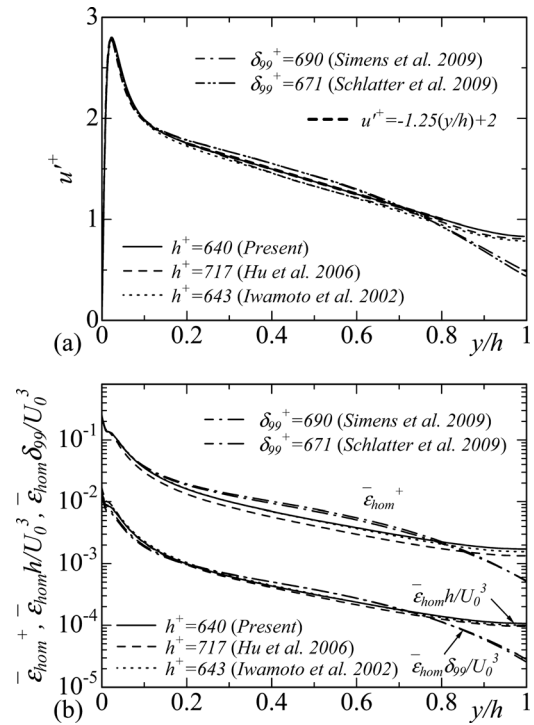


FIG. 13. Comparisons for u' and $\bar{\epsilon}_{hom}$ between the channel flow and the boundary layer: (a) u^+ ; (b) $\bar{\epsilon}_{hom}$ normalized by either inner (u_τ^4/ν) or outer [U_0^3/h or U_0^3/δ_{99} (U_0 denotes either the mean centreline velocity or free-stream velocity)] variables.

also agree reasonably well with Eq. (44). This appears to be due to $\bar{\epsilon}^+$ being about 30% larger in a boundary layer than in a channel over the equilibrium region, although the magnitude of u^+ is nearly the same in the two flows. A comparison of DNS data for u' and $\bar{\epsilon}_{hom}$ ($\equiv \overline{vu_{ij}^2}$) (the homogeneous energy dissipation rate) between the channel flow (Abe *et al.*,²⁶ Hu *et al.*,³¹ and Iwamoto *et al.*⁵⁰) and the boundary layer (Simens *et al.*³³ and Schlatter *et al.*³⁴) at comparable h^+ and δ_{99}^+ seems to confirm this (see Fig. 13 and also the comparison of u^+ by Jiménez and Hoyas⁵¹). Note that the fall-off in the u' and $\bar{\epsilon}_{hom}$ distributions for the turbulent boundary layer at $y/\delta_{99} > 0.7$ is caused by the intermittency associated with the turbulent/non-turbulent interface. The implication is that for a given value of the Kármán number (h^+ or δ_{99}^+), the maximum value of $R_{\lambda 1}$ is larger for the channel flow than the boundary layer [see Fig. 12(a)]. This also suggests that the former flow may be a better candidate for examining the approach towards local isotropy than the latter.

VI. CONCLUSIONS

DNS databases in a turbulent channel flow with passive scalar transport ($h^+ = 180, 395, 640$, and 1020 , $Pr = 0.71$) are used to examine the normalized mean energy and scalar dissipation rates C_ϵ and $C_{\epsilon\theta}$ [viz., Eqs. (3) and (8)]. Particular attention is given to the outer region. The main conclusions are as follows.

An interesting feature of a fully developed turbulent channel flow is the existence of a region, which starts in the inner region and extends well into the outer region of the

channel. In this region, the ratios $P_k/\bar{\varepsilon}$ and $P_\theta/\bar{\varepsilon}_\theta$ are close to 1. The region $y^+ = 100$ to $y/h = 0.7$, where the equality $P_k/\bar{\varepsilon} = P_\theta/\bar{\varepsilon}_\theta = 1$ is satisfied closely and the magnitudes of the diffusion terms are negligible, can be appropriately described as a near-equilibrium region, at least for $h^+ = O(10^2) \sim (10^3)$. In this region, $\bar{\varepsilon}$ and $\bar{\varepsilon}_\theta$, normalized by u^3/L_{uu} and $u'\theta^2/L_{u\theta}$, viz., C_ε and $C_{\varepsilon\theta}$, are approximately equal. Their magnitudes are about 2 and 1 in the logarithmic and outer regions, respectively, when the Kármán number h^+ is sufficiently large. The former magnitude, which is identical with that of $\bar{\varepsilon}_y/u_\tau^3$ or $\bar{\varepsilon}_\theta y/u_\tau T_\tau^2$ and hence with κ_u^{-1} or κ_θ^{-1} , tends to be approximately the same for the channel, pipe, and boundary layer. This reflects the similarity between the mean velocity and temperature distributions among these three canonical flows. When the Kármán number is large, these distributions should be relevant to the log-law (see, for example, Nagib and Chauhan⁵² and Marusic *et al.*⁵³). The latter magnitude is, on the other hand, about twice as large as in homogeneous isotropic turbulence due mainly to the existence of large-scale u structures in the outer region of the channel. In the present flow, the effect of R_{λ_1} and S^* on the magnitudes of C_ε and $C_{\varepsilon\theta}$ is less important than that of L_{uu} . Replacing L_{uu} by $L_{\theta\theta}$ in $C_{\varepsilon\theta}$ (viz., $C_{\varepsilon\theta_1}$) reduces the magnitude by a factor of about two, reflecting the smaller extent of the large-scale θ structures relative to the large-scale u structures. It should also be noted that the similarity between C_{ε_1} [Eq. (29)] and $C_{\varepsilon\theta_1}$ [Eq. (26)] in Fig. 7 is another consequence of the spectral analogy between q and θ .

The normalized parameters are also of importance from a turbulence model standpoint. In this context, C_{ε_2} [Eq. (31)], which is identical with C_D and C_{μ} , is ~ 0.1 over the equilibrium region. This mainly reflects the adequacy of the current turbulence models for the present flow. There is also a near equality between either C_ε and $C_{\varepsilon\theta}$ or between C_{ε_1} and $C_{\varepsilon\theta_1}$ in the near-equilibrium range, which has an important implication for the time scale ratio R , viz., R can be approximated with Eq. (34), without any information being required about the scalar field, when the analogy between velocity and scalar fields is reasonable ($Pr \approx 1$). The magnitude of R , however, increases slowly with increasing Pr in the outer region, and this needs to be taken into account when formulating R . Whilst the current $k_\theta - \varepsilon_\theta$ model (e.g., Nagano and Kim²⁰ and Yoshizawa²¹), which used R in Eq. (14), gives reasonable predictions, a formula of R may be useful for developing the eddy diffusivity model since it would allow the scalar time scale to be excluded from Eq. (14) and the resulting κ_r model would then satisfy the linearity principle of the scalar transport (Pope⁴⁴).

It should be noted that the equality between C_ε and $C_{\varepsilon\theta}$ also leads to a simple relationship between λ_1 and λ_θ , viz., Eq. (37). Note that Eq. (37) is likely to be applicable at least for $Pr = 0.71$ –10 (viz., air and water), the latter Pr range being larger than that for Eq. (34). This equality can in turn be used to establish analogous expressions for the dependence on h^+ of R_{λ_1} and Pe in the outer region. The proposed formulations for R_{λ_1} and Pe , as given by Eqs. (38) and (39) and also Eqs. (42) and (43), should be quite accurate for the channel flow (see Figs. 11 and 12). As shown in Fig. 12(a),

similar formulations with slightly different numerical constants should however be used in the boundary layer since the magnitude of R_{λ_1} is about 30% larger in the channel flow than in the boundary layer for the same Kármán number (h^+ or δ_{99}^+) due to $\bar{\varepsilon}^+$ being larger in the latter flow by nearly the same amount. The energy dissipation rate in a pipe flow is presumably closer to that in a channel flow than in a boundary layer since in the outer region there seems to be some structural similarity between the channel and pipe but not between the channel (or pipe) and the boundary layer (see Monty *et al.*⁵⁴). The formulations established for a channel flow should hence be applicable to a pipe flow.

ACKNOWLEDGMENTS

Computations performed on JAXA (Japan Aerospace Exploration Agency) Supercomputer System are gratefully acknowledged. H.A. was partially supported by the Ministry of Education, Culture, Sports, Science and Technology of Japan, Grant-in-Aid for Young Scientists (B), Grant No. 20760125, 2009 and also the NORDITA-KTH research program on the turbulent boundary layer in 2010. R.A.A. acknowledges the support of the Australian Research Council.

- ¹G. I. Taylor, "Statistical theory of turbulence," *Proc. R. Soc. London, Ser. A* **151**, 421 (1935).
- ²A. N. Kolmogorov, "Dissipation of energy in the locally isotropic turbulence," *Dokl. Akad. Nauk SSSR* **32**, 19 (1941) [reprinted in *Proc. R. Soc. London, Ser. A* **434**, 15 (1991)].
- ³K. R. Sreenivasan and R. A. Antonia, "The phenomenology of small-scale turbulence," *Annu. Rev. Fluid Mech.* **29**, 435 (1997).
- ⁴B. R. Pearson, T. A. Yousef, N. E. L. Haugen, A. Brandenburg, and P.-Å. Krogstad, "The 'zeroth law' of turbulence in steady isotropic turbulence," in *15th Australasian Fluid Mechanics Conference*, edited by M. Behnia, W. Lin, and G. D. McBain (The University of Sydney, Australia, 2004), paper N. AFMC00040.
- ⁵G. K. Batchelor, *The Theory of Homogeneous Turbulence* (Cambridge University Press, Cambridge, England, 1953).
- ⁶K. R. Sreenivasan, "On the scaling of the turbulence energy dissipation rate," *Phys. Fluids* **27**, 1048 (1984).
- ⁷K. R. Sreenivasan, "The energy dissipation in turbulent shear flows," in *Symposium on Developments in Fluid Dynamics and Aerospace Engineering*, edited by S. M. Deshpande, A. Prabhu, K. R. Sreenivasan, and P. R. Viswanath (Interline, Bangalore, India, 1995), pp. 159–190.
- ⁸K. R. Sreenivasan, "An update on the energy dissipation rate in isotropic turbulence," *Phys. Fluids* **10**, 528 (1998).
- ⁹J. L. Lumley, "Some comments on turbulence," *Phys. Fluids* **A4**(2), 203 (1992).
- ¹⁰U. Frisch, *Turbulent Flows* (Cambridge University Press, Cambridge, England, 1995).
- ¹¹Y. Kaneda, T. Ishihara, M. Yokokawa, K. Itakura, and A. Uno, "Energy dissipation rate and energy spectrum in high resolution direct numerical simulations of turbulence in a periodic box," *Phys. Fluids* **15**, L21 (2003).
- ¹²R. A. Antonia, T. Zhou, and G. Romano, "Small-scale turbulence characteristics of two-dimensional bluff body wakes," *J. Fluid Mech.* **459**, 67 (2002).
- ¹³R. A. Antonia and B. Pearson, "Effect of initial conditions on the mean energy dissipation rate and the scaling exponent," *Phys. Rev. E* **62**, 8086 (2000).
- ¹⁴P. Burattini, P. Lavoie, and R. A. Antonia, "On the normalized turbulent energy dissipation rate," *Phys. Fluids* **17**, 098103 (2005).
- ¹⁵S. Goto and J. C. Vassilicos, "The dissipation rate coefficient of turbulence is not universal and depends on the internal stagnation point structure," *Phys. Fluids* **21**, 035104 (2009).
- ¹⁶G. Xu, R. A. Antonia, and S. Rajagopalan, "Scaling of mean temperature dissipation rate," *Phys. Fluids* **12**, 3090 (2000).

- ¹⁷T. Watanabe and T. Gotoh, "Inertial-range intermittency and accuracy of direct numerical simulation for turbulence and passive scalar turbulence," *New J. Phys.* **6**, 1 (2004).
- ¹⁸D. A. Donzis, K. R. Sreenivasan, and P. K. Yeung, "Scalar dissipation rate and dissipative anomaly in isotropic turbulence," *J. Fluid Mech.* **532**, 199 (2005).
- ¹⁹B. J. McKeon and J. F. Morrison, "Asymptotic scaling in turbulent pipe flow," *Philos. Trans. R. Soc. London, Ser. A* **365**, 771 (2007).
- ²⁰Y. Nagano and C. Kim, "A two-equation model for heat transport in wall turbulent shear flows," *ASME J. Heat Transfer* **110**, 583 (1988).
- ²¹A. Yoshizawa, "Statistical modelling of passive-scalar diffusion in turbulent shear flows," *J. Fluid Mech.* **195**, 541 (1988).
- ²²S. Hoyas and J. Jiménez, "Reynolds number effects on the Reynolds-stress budgets in turbulent channels," *Phys. Fluids* **20**, 101511 (2008).
- ²³J. Kim and R. A. Antonia, "Isotropy of the small scales of turbulence at low Reynolds number," *J. Fluid Mech.* **251**, 219 (1993).
- ²⁴R. A. Antonia and J. Kim, "A numerical study of local isotropy of turbulence," *Phys. Fluids* **6**(2), 834 (1994).
- ²⁵H. M. Blackburn, N. N. Mansour, and B. J. Cantwell, "Topology of fine-scale motions in turbulent channel flow," *J. Fluid Mech.* **310**, 269 (1996).
- ²⁶H. Abe, R. A. Antonia, and H. Kawamura, "Correlation between small-scale velocity and scalar fluctuations in a turbulent channel flow," *J. Fluid Mech.* **627**, 1 (2009).
- ²⁷R. A. Antonia, H. Abe, and H. Kawamura, "Analogy between velocity and scalar fields in a turbulent channel flow," *J. Fluid Mech.* **628**, 241 (2009).
- ²⁸H. Abe, H. Kawamura, and Y. Matsuo, "Surface heat-flux fluctuations in a turbulent channel flow up to $Re_\tau = 1020$ with $Pr = 0.025$ and 0.71 ," *Int. J. Heat Fluid Flow* **25**, 404 (2004).
- ²⁹N. Kasagi, Y. Tomita, and A. Kuroda, "Direct numerical simulation of passive scalar field in a turbulent channel flow," *ASME J. Heat Transfer* **114**, 598 (1992).
- ³⁰J. Kim and P. Moin, "Transport of passive scalars in a turbulent channel flow," in *Turbulent Shear Flows*, edited by J.-C. André, J. Cousteix, F. Durst, B. E. Launder, F. W. Schmidt, and J. H. Whitelaw (Springer-Verlag, Berlin, Germany, 1989), Vol. 6, pp. 85–96.
- ³¹Z. W. Hu, C. L. Morfey, and N. D. Sandham, "Wall pressure and shear stress spectra from direct numerical simulations of channel flow," *AIAA J.* **44**(7), 1541 (2006).
- ³²P. R. Spalart, "Direct simulation of a turbulent boundary layer up to $Re_\theta = 1410$," *J. Fluid Mech.* **187**, 61 (1988).
- ³³M. P. Simens, J. Jiménez, S. Hoyas, and Y. Mizuno, "A high-resolution code for turbulent boundary layers," *J. Comp. Phys.* **228**, 4218 (2009).
- ³⁴P. Schlatter, R. Örlü, Q. Li, G. Brethouwer, J. H. M. Fransson, A. V. Johansson, P. H. Alfredsson, and D. S. Henningson, "Turbulent boundary layers up to $Re_\theta = 2500$ studied through simulation and experiment," *Phys. Fluids* **21**, 051702 (2009).
- ³⁵G. Comte-Bellot, "Contribution à l'étude de la turbulence de conduite," Ph. D. thesis (University of Grenoble, France, 1963) (trans. P. Bradshaw ARC 31 609 FM 4102, 1969).
- ³⁶N. Hutchins and I. Marusic, "Evidence of very long meandering features in the logarithmic region of turbulent boundary layers," *J. Fluid Mech.* **579**, 1 (2007).
- ³⁷J. P. Monty and M. S. Chong, "Turbulent channel flow: Comparison of streamwise velocity data from experiments and direct numerical simulation," *J. Fluid Mech.* **633**, 461 (2009).
- ³⁸P. Bradshaw, "The turbulence structure of equilibrium boundary layers," *J. Fluid Mech.* **29**, 625 (1967).
- ³⁹N. Kasagi and Y. Ohtsubo, "Direct numerical simulation of low Prandtl number thermal field in a turbulent channel flow," in *Turbulent Shear Flows*, edited by F. Durst, R. Friedrich, B. E. Launder, F. W. Schmidt, U. Schumann, and J. H. Whitelaw (Springer, Berlin, Germany, 1993), Vol. 8, pp. 97–119.
- ⁴⁰H. Kawamura, K. Ohsaka, H. Abe, and K. Yamamoto, "DNS of turbulent heat transfer in channel flow with low to medium-high Prandtl number fluid," *Int. J. Heat Fluid Flow* **19**, 482 (1998).
- ⁴¹H. Kawamura, H. Abe, and Y. Matsuo, "DNS of turbulent heat transfer in channel flow with respect to Reynolds and Prandtl number effects," *Int. J. Heat Fluid Flow* **20**, 196 (1999).
- ⁴²F. Schwertfirm and M. Manhart, "DNS of passive scalar transport in turbulent channel flow at high Schmidt numbers," *Int. J. Heat Fluid Flow* **28**, 1204 (2007).
- ⁴³M. Kozuka, Y. Seki, and H. Kawamura, "DNS of turbulent heat transfer in a channel flow with a high spatial resolution," *Int. J. Heat Fluid Flow* **30**, 514 (2009).
- ⁴⁴S. B. Pope, "Consistent modeling of scalars in turbulent flows," *Phys. Fluids* **26**, 404 (1983).
- ⁴⁵T. Wei and W. W. Willmarth, "Reynolds-number effects on the structure of a turbulent channel flow," *J. Fluid Mech.* **204**, 57 (1989).
- ⁴⁶B. J. Balakumar and R. J. Adrian, "Large- and very-large-scale motions in channel and boundary-layer flows," *Philos. Trans. R. Soc. London* **365**, 665 (2007).
- ⁴⁷J. P. Monty, "Developments in smooth wall turbulent duct flows," Ph. D. thesis (University of Melbourne, Australia, 2005).
- ⁴⁸N. Hutchins, T. B. Nickels, I. Marusic, and M. S. Chong, "Hot-wire spatial resolution issues in wall-bounded turbulence," *J. Fluid Mech.* **635**, 103 (2009).
- ⁴⁹S. G. Saddoughi and S. V. Veeravalli, "Local isotropy in turbulent boundary layers at high Reynolds number," *J. Fluid Mech.* **268**, 333 (1994).
- ⁵⁰K. Iwamoto, Y. Suzuki, and N. Kasagi, "Reynolds number effect on wall turbulence: Toward effective feedback control," *Int. J. Heat Fluid Flow* **23**, 678 (2002).
- ⁵¹J. Jiménez, and S. Hoyas, "Turbulent fluctuations above the buffer layer of wall-bounded flows," *J. Fluid Mech.* **611**, 215 (2008).
- ⁵²H. M. Nagib and K. A. Chauhan, "Variations of von Kármán coefficient in canonical flows," *Phys. Fluids* **20**, 101518 (2008).
- ⁵³I. Marusic, B. J. McKeon, P. A. Monkewitz, H. M. Nagib, A. J. Smits, and K. R. Sreenivasan, "Wall-bounded turbulent flows at high Reynolds numbers: Recent advances and key issues," *Phys. Fluids* **22**, 065103 (2010).
- ⁵⁴J. P. Monty, N. Hutchins, H. C. H. Ng, I. Marusic, and M. S. Chong, "A comparison of turbulent pipe, channel and boundary layer flows," *J. Fluid Mech.* **632**, 431 (2009).